Renewable and Sustainable Energy Reviews 112 (2019) 183–194

Contents lists available at ScienceDirect

Renewable and Sustainable Energy Reviews

journal homepage: www.elsevier.com/locate/rser

Enhancing the performance of automotive radiators using nanofluids

Zafar Said[a,*], M. El Haj Assad[a], Ahmed Amine Hachicha[a], Evangelos Bellos[b], Mohammad Ali Abdelkareem[a,c], Duha Zeyad Alazaizeh[a], Bashria A.A. Yousef[a]

[a] Department of Sustainable and Renewable Energy Engineering, University of Sharjah, United Arab Emirates
[b] Thermal Department, School of Mechanical Engineering, National Technical University of Athens, Greece
[c] Chemical Engineering Department, Minia University, Elminia, Egypt

ARTICLE INFO

Keywords:
Nanofluids
Automotive radiator
Heat transfer
Thermophysical properties
Stability
Corrosion

ABSTRACT

Advanced heat removal technologies are critical for high-performance automotive engines. The conventional fluids being used today are based on a mixture of distilled water (DW) and ethylene glycol (EG), which widens the operational temperature range but at the same time limits the heat removal. Therefore, the use of nanofluids for improving heat transfer performance has soared over the past few years. The problem is that most of the reports highlight the short-term heat transfer results which may not be true over time. In this paper, a suggested best practice for analyzing the usage of nanofluids in heat transfer applications is presented, specifically for an actual car radiator. This work investigates the use of aluminum oxide (Al_2O_3) and titanium dioxide (TiO_2) nanoparticles dispersed in DW and EG at 50:50 volumetric proportions. The choice of these oxide-based nanofluids is motivated by their anti-corrosive properties that are usually not analyzed or discussed in most of the articles. Furthermore, the emphasis is given on the presentation of a comprehensive characterization of the nanofluids including thermophysical properties (size, density, viscosity, thermal conductivity, corrosive behavior) and long-term stability (zeta potential) which are essential for an end-user to have. The results showed a maximum enhancement of the thermal performance by 24.21% using Al_2O_3 at a volume fraction of 0.3%. Friction factor and performance evaluation criterion (PEC) for the radiator experiments are calculated in order to determine the penalty in the pressure drop and to evaluate it properly. Finally, it is found that the values of PEC lie in the range of 1.03–1.31 which indicates significant flow enhancement.

1. Introduction

The improvement in automotive technologies has led to increased thermal loads, and therefore higher cooling rates are required [1]. The addition of fins, microchannel, and turbulators are the traditional approaches used to increase cooling rates of the radiator which are already extended to their limits [1,2]. In recent years, the automotive industry has been focused on the weight reduction of the vehicle as it improves the fuel economy and the associated running costs [3]. Weight reduction can be achieved in the engine cooling system. Furthermore, many conventional coolants (lubricants and water) have characteristically shown poor heat transfer properties due to their lower thermal conductivities (TCs) [1,4]. Engine performance, fuel efficiency, and emissions are specific parameters of an automobile which are profoundly affected by convective heat transfer [5,6]. Therefore, a new compact and innovative coolants and/or coolant systems are needed to fulfill the growing needs for heat removal in a clean and eco-friendly way [7].

Nanofluids (NF) have a huge ability to enhance automotive and heavy-duty engine cooling rates, reducing the weight and lowering the complexity of thermal management systems [2,3,5,7,8]. NFs are known to have higher TCs and heat transfer coefficients compared to the conventional fluids due to their larger surface area and a large number of atoms present on the surface of the nanoparticles [3,5,9,10]. Many researchers have suggested that one of the main parameters resulting in the enhancement of heat transfer is the Brownian motion. Brownian motion is caused by the slight perturbations in temperature and velocity formulation as suggested by Xuan and Roetzel [11]. The random motion of the nanoparticles suspended in the fluid cause thermal boundary layer thickness to shrink, which has a significant contribution to such heat transfer enhancement [5,12]. The random motion of the nanoparticles would result in creating a slip velocity between the particles and the fluid medium [13,14]. Furthermore, these nanoparticles may reduce corrosion and erosion dramatically due to their small size [15]. These fluids have already been used for various automotive applications such as coolants, fuel additives, lubricants, shock absorbers and

* Corresponding author.
E-mail addresses: zsaid@sharjah.ac.ae, zaffar.ks@gmail.com (Z. Said).

https://doi.org/10.1016/j.rser.2019.05.052
Received 14 December 2018; Received in revised form 17 March 2019; Accepted 23 May 2019
Available online 30 May 2019

Nomenclature

$\mathbf{A_t}$	Tube area, $A_t = W_t H_t$ (m^2)
$\mathbf{A_{t,\ total}}$	Total area of the tube, $A_{t,\ total} = N_t A_t$ (m^2)
$\mathbf{c_p}$	Specific heat ($J.kg^{-1}.K^{-1}$)
$\mathbf{C_r}$	Heat capacity ratio
$\mathbf{D_h}$	Hydraulic Diameter $D_h = \frac{4A_t}{P_t}$ (m)
d_p	Diameter of nanoparticle (nm)
$\mathbf{H_r}$	Radiator height (m) Friction coefficient
g	Gravity force ($m.s^{-2}$)
k	Thermal Conductivity($W.m^{-1}.K^{-1}$)
$\mathbf{L_r}$	Radiator length (m)
$\dot{m}$	Mass flow rate ($kg.s^{-1}$)
$\mathbf{N_t}$	Number of tubes
NTU	Number of heat transfer units Nusselt Number
$\mathbf{P_t}$	Wetted Perimeter, $P_t = 2W_t + 2H_t$ (m)
$\dot{q}$	Predicted heat transfer rate (W)
$\dot{q}_{max}$	Maximum heat transfer rate (W)
r	Radius (m)
V	Flow velocity ($m.s^{-1}$)
$\dot{V}$	Volumetric flow rate ($m^3.s^{-1}$)
$\mathbf{W_t}$	Tube width (m)

Subscripts

bf	Base-fluid
f	Fin
nf	nanofluid
p	Particle
r	Radiator
t	Tube

Greek Symbol

α	Diffusivity ($m^2.s^{-1}$)
ε	Effectiveness
ϑ	Sedimentation velocity of nanoparticles ($m.s^{-1}$)
μ	Viscosity ($kg.m^{-}1.s^{-1}$)
ρ	Density ($kg.m^{-3}$)
φ	The volume fraction of nanoparticles
Ψ	Shape factor
ζ	Zeta Potential

Abbreviations

DW	Distilled water
EG	Ethylene glycol
NF	Nanofluid
PEC	Performance evaluation criterion
PVP	Polyvinylpyrrolidone
TC	Thermal conductivity

refrigerants [5,16]. Based on past reviews [2,5,7,17], TC is not the only critical impact of the nanoparticles suspension to basefluid, but also the dynamic viscosity plays a vital role as well [18]. However, the high volume fractions of nanoparticles-in-fluids results in higher viscosity as well as increased pumping power which is one of the main drawbacks that restricts their widespread use in heat transfer applications [19,20]. Nevetherless, the increase in the viscosity has to be more than four times larger than the comparable increase in TC for NF to be not beneficial at all [21,22]. Furthermore, the long-term stability of the NF mixture is another concern as it does have a direct effect on the constancy of the TC [13,23].

Table 1 includes all the found studies, and their characteristics are summarized in this table. More specifically, the NF type (nanoparticle and base fluid), the nanoparticle diameter, the concentration, the preparation technique, the type of the surfactant and the important outcomes of every study are given in this table.

While analyzing the recent literature on the use of NFs, one can classify the published reports into two categories; one is mostly focused on the thermophysical properties of the fluids [7,34–37], and another presents the resulting outcomes directly for a given application [38–41]. However, from the application point of view, it is clear that short-term results of NFs, while promising, can be different on the long-term. This is because of the lack of a comprehensive analysis of the used NF for that application. For example, Leong et al. [42] used EG with 2% volume fraction of copper NF and reported enhancement in the overall heat transfer coefficient and bulk heat transfer by 3.8% compared to the basefluid. They also showed a reduction in the frontal air area by 18.7% for Reynolds number of 6000 and 5000 for air and coolant respectively. Heris et al. [43] extended the study using 0.8 vol % CuO in EG/water and found 55% of heat transfer enhancement compared to the basefluid. It is known that such materials suspended in the basefluid will endure corrosion problems in the pipe system on the long-term, resulting in a decrease in the performance and lifetime [44]. There are many reports about the ability of NFs to be used as a coolant in the literature as summarized in Table 2, but this data lacks the experimental results about the appropriateness of using NFs in cooling systems and its effect on the metal surfaces. This is a one-sided view of the performance of such NFs, and a more comprehensive analysis is necessary.

Therefore, this paper aims to suggest best practice guidelines to properly present the performance of a NF in a car radiator. More specifically, this work investigates the forced convection heat transfer coefficients for a DW and EG at 50:50 vol mixture fluid without and with Al_2O_3 and TiO_2 nanoparticles. The effects of the operating conditions on the heat transfer performance using these fluids are analyzed. These NFs are examined from many points of view by taking into consideration the stability and corrosion problems, as well as the thermophysical properties and their effect on heat transfer enhancement results. Hence, this study emphasizes the importance of a detailed investigation of a NF that includes stability, thermophysical properties, corrosion, heat transfer, Nusselt number, friction factor, and performance evaluation criterion (PEC) from laminar flow to turbulent flow, to assess the short and long-term performance of the medium appropriately.

2. Materials and methods

2.1. Materials

Two types of nanoparticles were used in this work: aluminum oxide Al_2O_3 and titanium oxide TiO_2 which were both purchased from Nanostructured & Amorphous Materials Inc. (NanoAmor), USA. The main reason for choosing these nanoparticles is low cost and non-toxic. The chemical and physical properties of these nanoparticles are given in Table 3. The basefluid used in this study consisted of a mixture of DW and EG (from Fluka Analytical). Two types of surfactants are used in this study, one is a nonionic polymer of Polyvinylpyrrolidone (PVP), whereas the other is anionic material of Arabic gum (AG) acquired from Sigma Aldrich, Germany.

2.2. Preparation and characterization of NFs

The TiO_2 and Al_2O_3 NFs were prepared by two-step method by dispersing different volume fractions, i.e., 0.05% and 0.3% in the

Table 1
Summary of literature related to the stability of metal oxide NFs.

Researcher (Year)	NP Type and Size	Base Fluid	φ (%)	Process	Technique	Time, T and pH	Type of Surfactant and Ratio	Important Outcomes
Das et al. [24] (2016)	TiO_2 (21 nm)	DW	0.1–2.0	Two-step method	Ultrasonic bath (Misonix, 40 kHz)	2 h 30 °CpH = 3.9–4.9 and 2.8–3.7	Cetyltrimethylammonium bromide (CTAB) and AA 1:10	Stable for several days (500 h)
Said et al. [25] (2015)	TiO_2 (21 nm)	DW	0.1, 0.3	Two-step method	High pressure homogenizer	30 cycles	Polyethylene glycol 400–1:2	Stable for 30 days, ζ-value = 41.8 mV
Khairul et al. [26] (2016)	CuO (30–50 nm)	DW	0.05–0.15	Two-step method	–	pH = 8.50–9	Sodium dodecylbenz-enesulfonate 0.15%	Stable, ζ-value = 85.1 mV
	Al_2O_3 (10 nm)	DW	0.05–0.15	Two-step method	–	pH = 7.50–8	sodium dodecylbenz-enesulfonate 0.15%	Stable, ζ-value = 72.2 mV
Witharana et al. [27] (2013)	TiO_2 (21 nm)	DW/EG 50:50	1	Two-step method	Digital Sonicator (37 kHz)	24 h pH = 6.2–7.8	Without surfactant	Stable, ζ-value = −40 mV. Isoelectric point at pH = 4.7
	Al_2O_3 (13 nm)	DW/EG 50:50	1	Two-step method	Digital Sonicator (37 kHz)	16 h pH = Less than 6	Without surfactant	Stable for 2 months, ζ-value = 100 mV. The isoelectric point at pH = 9.5
	ZnO (40–50 nm)	PEG	1	Two-step method	Digital Sonicator (37 Hz)	4 h pH = 9	Without surfactant	Stable
Li et al. [28] (2008)	Cu (25 nm)\	DW	0.05	Two-step method	Ultrasonic Cleanser (40 kHz, 100 W)	1 h 25–30 °C pH = 8.5–9.5	sodium dodecylbenzene sulfonate	Stable, ζ-value between −40 and −45 mV. The surface charge increases when the pH goes far away from the IEP, so the particles get stable
Goudarzi and Jamali [29] (2017)	Al_2O_3 (40 nm)\	EG	0.08, 0.5, 1	Two-step method	Ultrasonic vibration (24 kHz,400 W)	1 h	sodium dodecylbenzene sulfonate	Not stable
Naik et al. [30] (2010)	Cu (Less than 50 nm)	PEG/DW 60:40	0.025, 0.1, 0.4, 0.8, 1.2	Two-step method	Ultrasonic method	–	Without surfactant	No sediment until 6 h after the ultra-sonication process.
Kim et al. [31] (2009)	Au-NPs (40–130 nm)	DW	0.002–5	One -Step method	Ultrasonic-wave (160kw) irradiation condition (40 kHz)PLAL (laser irradiation conditions).	6 h pH = 4 9 h	Without surfactant	Stable, ζ-value = -38 mV
Abdul et al. [32] (2016)	TiO_2(50 nm)	DW/EG 60:40	0.5–1.5	Two-step method	Ultrasonic bath (37 kHz,80w)	2 h	Without surfactant	Stable for 3 months
Michał et al. [33] (2012)	CuO(30–50 nm)	DW	1	Two-step method	ultrasonic mixerSonix (20 kHz, 130 W,123 μm)	–	Sodium hexametafosfate (1% mass ratio)	Stable, ζ-value = -60.2 mV

Table 2
Summary of studied NFs for enhancement of car radiators performance.

Reference (Year)	Nanofluid	Particles Size (nm)	Φ (%)	T (°C)	Properties	k_{nf} ($W.m^{-1}.K^{-1}$)	Findings
Leong et al. [42] (2010)	CuO- EG	–	0–2	70–95	k, C_p, μ, ρ	3.8%	NFs showed improved heat transfer of 3.8%.
Heris et al. [43] (2014)	CuO (EG-W) (40–60%)	60	0.05–0.8	35–54	k, C_p, μ, ρ	–	55% enhanced heat transfer at 0.8 vol% of CuO suspended in EG/DW.
Naraki et al. [45] (2013)	CuO- water	60	0.04–0.4	50–80	k, C_p, μ, ρ	–	8% improvement in overall heat transfer at 0.4 vol% of CuO nanoparticles.
Bigdeli et al. [3] (2016)	–	–	–	–	k, C_p, μ, ρ	–	Advantages of using NFs as coolants for the automotive radiator and some guidelines have been suggested for their rational design and usage.
Li et al. [46] (2016)	SiC- (EG-W) (40–60%)	30	0.1–0.5	10–50	k, μ	53.81%	SiC based NFs showed improved overall effectiveness of 1.6 using NFs (0.2 vol%).
Devireddy et al. [47] (2016)	TiO_2– (EG-W) (40–60%)	21	0.1–0.5	30–40	k, μ	3%	35% enhancement in heat transfer is obtained at the concentration of 0.5%. Higher volume fractions improves heat transfer.
Zhao et al. [6] (2016)	TiO_2, Al_2O_3, CuO, SiO_2			20–80	k, μ	–	Addition of nanoparticles improved the heat transfer and pressure. The increase in pressure drop could limit the efficiency factor of the automotive radiator.
Elsebay et al. [48] (2016)	Al_2O_3-water, CuO-water	–	1–7	–	k, C_p, μ, ρ	–	Increasing the nanoparticles increases the pumping power and heat transfer. Al_2O_3 showed better heat transfer enhancement and lower pumping power compared to CuO.
Sidik et al. [8] (2017)	–	–	–	–	k, C_p, μ, ρ	–	A review on the application of NFs for cooling engine automotive.
Chiam et al. [49] (2017)	Al_2O_3- (EG-W) (40–60%)	13	0.2–1	30–70	k, μ	12.8%	The maximum dynamic enhanced up to 50% for 60:40 (DW: EG).
Gulhane and Chincholkar [50] (2017)	Al_2O_3- water	50	0.1–0.4	50–70	k, C_p, μ, ρ	–	For 0.4 vol %, the convection heat transfer coefficient enhanced by 45.87%. Higher volume fractions resulted in further improvement in heat transfer.
Hatami et al. [51] (2017)	CuO, TiO_2, Al_2O_3, Fe_3O_4	–	–	80	k	–	Results showed that TiO_2 and CuO have better results than Al_2O_3 and Fe_3O_4.
Hussein et al. [52]. (2014)	TiO_2	100	1–4	60–90	k, C_p, μ, ρ	20%	TiO_2 NFs showed enhanced in hydrodynamic flow and heat transfer enhancement, which could be used for industrial applications as well.
Oliveira, Contreras et al. [53] (2017)	MWCNT – water	100 nm	0.05–0.16%	50–80	k, μ, ρ	17%	Higher volume fraction results in higher heat transfer enhancements of NFs.
Selvam, Lal et al. [54] (2017)	GnP	10 nm	0.1–0.5%	35–45	k, C_p, μ, ρ	29%	Heat transfer coefficient is enhanced by 29% at a particle loading of 0.5 vol% using Graphene nanoplatelet.

Table 3
Physical, morphological and thermal properties of TiO_2 and Al_2O_3 nanoparticles.

Properties	Titanium Oxide TiO_2	Aluminum Oxide Al_2O_3
Color	White	White
Particle size	5 nm	10 nm
Purity	99.8%	99.99%
Morphology of Particles	Spherical	Spherical
Form	Powder	Powder
Density (g.cm^{-3})	3.9	3.9
Thermal conductivity (W.m^{-1}.K^{-1})	8.7 [55]	40 [55]
Specific heat (kJ.kg^{-1}.K^{-1})	689 [55]	880 [56]

mixture of DW and EG which was stirred for 30 min using a magnetic stirrer followed by sonication using an ultrasonic processor (UP400S, 400 W maximum power, 24 kHz frequency) for about 2 h with 0.5 duty cycles and 60% power amplitude heat transfer [5]. Such a technique provides the required uniform and homogenous nanosuspension and improves the stability of the NF. PVP and AG were used for stabilization of TiO_2 and Al_2O_3 NFs at different mass fractions. An analytical grade of 0.1 mol L^{-1} of NaOH was used to adjust the pH of the solution and control the stability of NFs. The stability of the NF was determined by measuring the zeta potential (ζ) of the nanofluid, which is the electric potential in the double layer at slipping plane relative to the point in the bulk fluid away from the interface and is a key indicator of colloidal stability. Therefore, the samples were evaluated using (Nanotrac Wave II Q, Microtrac Inc., Nikkiso America) for ζ and particle size measurement.

A KD2 Pro Thermal Properties Analyzer (Decagon Devices, Inc., acc. to ASTM D5334 and IEEE 442–1981 standards) was employed to measure the TC of the prepared NFs [57] in a range 20 °C–70 °C using a water bath. The device is equipped with a 6-cm long and 1.3-mm diameter KS-1 sensor probe. Once the desired temperature was reached, the sample was allowed to become thermally stable before taking the measurement (about 15 min). Ten values for each temperature were recorded, for which the average data is reported in the figure to have consistency. The viscosity and density of NFs were measured in the same temperature range using an Anton Paar, Lovis 2000 M/ME density and viscometer [58]. Density and viscosity data were repeated three times to have consistency in results. For the evaluation of the corrosive properties of the NFs, copper electrodes of 0.5 × 5 cm^2 were used, which were pre-cleaned with ethanol and deionized water, immersed in 0.5 M HCl. A three-electrode setup was used in which a saturated Calomel Electrode (SCE) served as a reference electrode and a platinum plate as a counter electrode. The measurement was carried out on a Biologic VSP-300 potentiostat connected to a PC with EC-Lab software.

2.3. Radiator setup

The radiator setup is shown in Fig. 1. The main components of the setup are the following:

1. Reservoir with 15 L storage capacity of the heat transfer fluid.
2. Heater and temperature controller (maximum temperature of 200 °C).
3. Volumetric gear pump (Micro diaphragm pump with 4 L min^{-1} maximum flow).
4. Flow rate control valve and flow rate meter (LTZ M – 15, max. 4 L min^{-1}).
5. Toyota Corolla 2006 model radiator with 2 L capacity at idle conditions (dimensions are given in Table 4).
6. K-type thermocouples fixed at different locations in the installation.

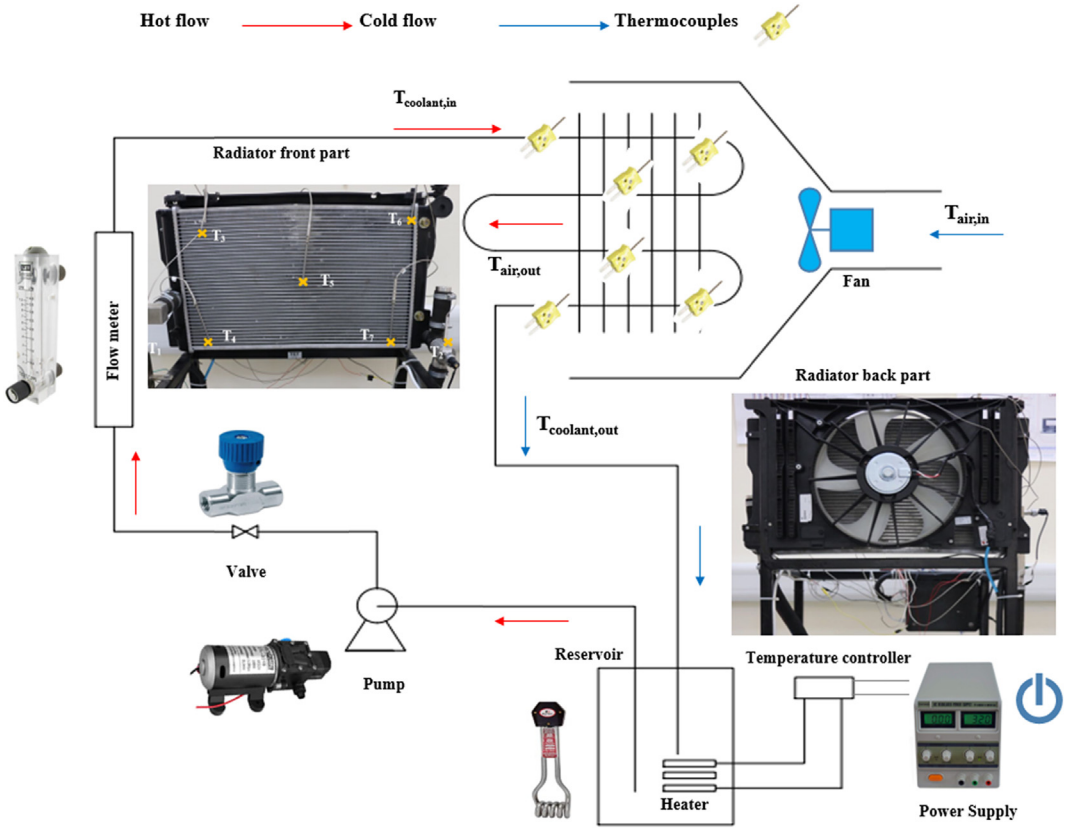

Fig. 1. Schematic presentation of the experimental setup for a Toyota Corolla 2006 radiator.

Table 4
Geometric characteristics of the car radiator.

Description	Specification
Radiator Length (L_r)	61 cm
Radiator Width (W_r)	6 cm
Radiator Height (H_r)	41 cm
Tube Width (W_t)	35 mm
Tube Height (H_t)	1 mm
Number of tubes (N_t)	36
Fin Length (L_f)	20 mm
Fin Height (H_f)	76 μm
Number of fins (N_f)	7600

2.4. Heat transfer calculations

The main purpose of the radiator is to decrease the temperature of the coolant fluid (see Fig. 1), which is computed using the ε-NTU method [59]. The heat transfer rate for each flow can be calculated using:

$$\dot{q} = \dot{m}_{air} C_{p,air} (T_{out,air} - T_{in,air}) = \dot{m}_{coolant} C_{p,coolant} (T_{in,coolant} - T_{out,coolant}) \quad (1)$$

where the specific heat of the coolant (NF) is obtained from Refs. [11,60]:

$$C_{pnf} = \frac{\varphi(\rho C_p)_p + (1-\varphi)(\rho C_p)_{bf}}{\rho_{nf}} \quad (2)$$

The definitions of the temperature are provided in Fig. 1. The parameter (ϕ) represents the volume fraction of the particles in the basefluid. In the experimental results the Nu number can be calculated using the following equation [61,62]:

$$Nu_{\exp} = \frac{h_{\exp} D_h}{k_{\exp}} = \frac{\dot{m} C_p (T_{coolant,in} - T_{coolant,out}) D_h}{A_s (T_b - T_w) k_{\exp}} \quad (3)$$

where $T_{coolant,\ in}$ and $T_{coolant,\ out}$ are the inlet and outlet temperatures of the coolant, respectively T_b is bulk mean temperature (the average of the inlet and outlet temperature) and T_w the outlet tube surface temperature (the average temperature of the seven temperatures recorded by thermocouples), D_h is the hydraulic diameter (m), $D_h = 4A_t/P_t$, A_t is the tube area, $A_t = W_t H_t$ and P_t is the Perimeter, $P_t = 2W_t + 2H_t$[62]. Reynolds number is calculated by the equation below [63]:

$$\mathrm{Re} = \frac{2\dot{m}}{(W_t + H_t)\mu} \quad (4)$$

where, $\mu$is dynamic fluid viscosity in $kg.s^{-1}.m^{-1}$

The coolant is pumped from the heater (simulates the engine in actual conditions) to the radiator to cool it down, and then the engine heats it due to heat released by the combustion process. The hot coolant flows through the radiator tubes which are linked to several fins as shown in (Fig. 1).

In the case of the pressure drop, the friction factor of the NFs compared to the base fluid does not change significantly with a low volume fraction of the nanoparticles under similar flow rate [64], however, if higher volume fractions are used it would affect the pumping power [5].

The friction factor, f_{nf} for laminar flow is calculated using Equation (5) which was correlated by Darcy-Weisbach [65], which is expressed as follows:

$$f_{nf} = 64/\mathrm{Re} \quad (5)$$

The friction factor, f_{nf} for turbulent flow is calculated using Equation (6) suggested by Filonenko [66], expressed as follows:

$$f_{nf} = (0.79 Ln\ \mathrm{Re}_{nf} - 1.69)^{-2} \quad (6)$$

An orderly error analysis was carried out to estimate the possible errors related with the heat transfer coefficient, Nusselt number, Reynolds number and friction factor using the approach suggested by Beckwith et al. [67]. The following uncertainties were obtained 0.22%, 0.25%, 0.3% and 0.3%, respectively.

The performance evaluation criteria (PEC) according to Webb [68] at a given pumping power is used to evaluate heat transfer improvement. The heat transfer enhancement is defined as: $E_{Nu} = N_{nf}/N_{bf}$, while the relative pressure drop penalty is given by $E_f = f_{nf}/f_{bf}$. In other words, PEC is the ratio of heat flow rate transferred for a given pumping power in a test section, which is written as combing these two dimensionless numbers as:

$$PEC = \frac{E_{Nu}}{E_f^{1/3}} \quad (7)$$

3. Results and discussions

3.1. Stability of TiO_2 NFs and Al_2O_3 NFs

The stability of NFs and the behavior of the nanoparticles in the basefluid has been a dilemma that has not been resolved completely up to date as each nanoparticle behaves and reacts differently to different base fluids [13,69]. The agglomeration of nanoparticles does not only result in the sedimentation and clogging but also decreases the thermal conductivity. Surfactants or dispersants are usually used to stabilize the NFs. Additions of surfactants lower the surface tension of the host fluids and increase the immersion of the nanoparticles [70]. From the detailed literature carried out in the introduction section, it can be said that the

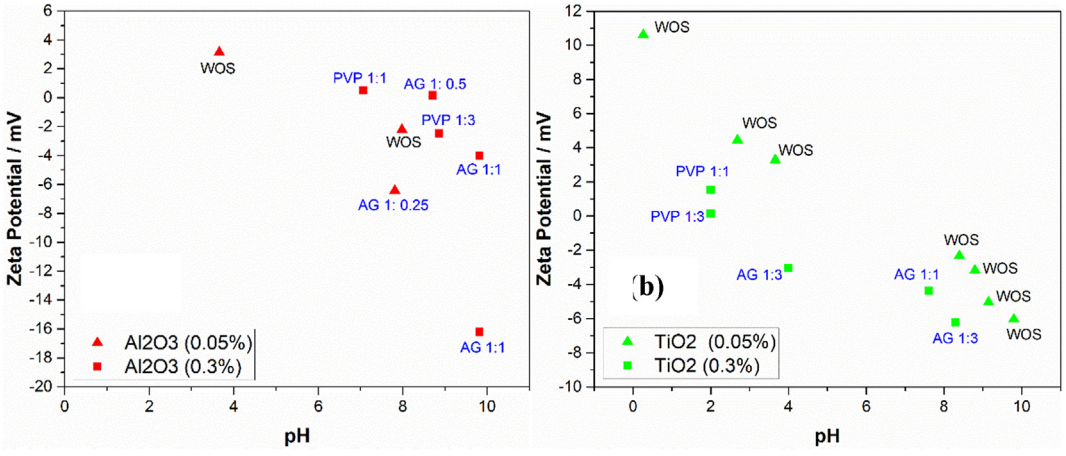

Fig. 2. Zeta potential values for a) Al_2O_3 NFs and b) TiO_2 NFs without surfactant (WOS) and with surfactants (AG and PVP at different ratios).

effect of surfactant addition on the stability and heat transfer characteristics of NFs are not well elucidated and prospected [71].

The stability of Al_2O_3 in a mixture of DW/EG for three volume concentrations: 0.05% and 0.3% were measured. Fig. 2a shows the results of stability for the examined samples. The best stability was found to be for the samples with AG surfactant with 0.05 and 0.3 vol%. The ζ-value is around 9.78 mV with a negative polarity which is considered the highest value at pH 9.81. Furthermore, PVP did not affect the ζ values for both 1:1 and 1:3 nanoparticles to PVP mass ratios, and the ζ value stayed close to the isoelectric point. PVP as a surfactant for Al_2O_3 has been used in literature for the stability of only DW or EG based NFs but no literature on using PVP for a mixture of DW and EG has been reported before [72,73].

The stability of TiO_2 nanoparticles in a mixture of DW/EG for 0.05 and 0.3 vol% and the results are presented in Fig. 2b. It can be seen from this figure that best results were found around 5 mV for 0.05 vol% and a pH of 9.15 with the addition of base and without any addition of surfactants. On the other hand, the results for 0.3% volume fraction show that the highest value for ζ is around 10 mV at pH 0.27 without any addition of base or surfactants which can be considered a little stable. The results also show that each of the PVP and AG surfactants give an adverse effect for both 1:1 and 1:3 nanoparticles to surfactant mass ratios. It seems that the stability will be better for 1:3 TiO_2 nanoparticles to AG mass ratio which increases the pH above 9 instead of 4. Titrations were performed for 0.05% and 0.3% volume concentrations of TiO_2 –DW/EG NFs to find the isoelectric points (IEP). The 0.05% volume concentration curve shows that the iso-electric points nearest to be between pH equals 8 and 9 which considered at this point the NF is unstable. While the 0.3% volume concentration curve shows that the nearest iso-electric points to be at pH equals 2, and the ζ becomes higher when the pH is more acidic.

3.2. Particle size analysis

Dynamic light scattering (DLS) method is used to determine the size of the particle by recording the changes in the intensity of light scattered from a NF. This technique indicates the average agglomerate size in the fluid. The larger particles present faster sediment than the smaller particles. This fact leads to a decrease in average particle size, and it has a significant influence on the stability of nanoparticle in the liquid. Fig. 3a shows the average particle size of Al_2O_3–DW/EG NFs for 0.05 and 0.3 vol% through a graphical illustration. For the 0.05% volume fraction, the average particle diameter was at 0.0683 μm (68.3 nm) while for 0.3 vol%, the average particle diameter was observed to be 0.086 μm (86 nm). The results of DLS show that the higher volume concentration of the nanoparticles had some influence on the size of particles as indicated in Fig. 3a below resulting in bigger average particle diameter for the higher volume concentration, which is due to agglomeration of the nanoparticles.

On the other hand, Fig. 3b shows the average particle size of TiO_2 -DW/EG NFs for 0.05 and 0.3 vol%. As observed from the figure, the TiO_2 NF with 0.3 vol% had an average particle diameter equal to 0.036 μm (36 nm). Whereas, the TiO_2 NF with 0.05% volume fraction had the average particle diameter equals 0.0064 μm (6.4 nm). On the other hand, higher volume fraction results in a bigger sized average particle diameter. Fig. 3a and b shows the inset photographs of the prepared NFs after 24 h.

3.3. Viscosity, density and thermal conductivities of NFs

Viscosities of Al_2O_3 and TiO_2 NF using two varying volume fractions were measured in the temperature range of 20 °C–70 °C and plotted in Fig. 4a. Moreover, to verify the accuracy of experimental results, the viscosity of basefluid was measured and compared with the ASHRAE standard [74]. Fig. 4a presents that the viscosity exponentially reduces with the rising temperature. Higher values of viscosity were observed for the NFs compared to the basefluid. With the additions of nanoparticles, the viscosity of the NFs increased as well. It is shown that TiO_2 NF has a higher viscosity than Al_2O_3 NF. Moreover, comparing with the literature [5,75–77] the viscosity should increase with a higher volume concentration of the particles and decrease with an increase in temperature which is consistent with the obtained pattern.

NF density depends on the nanoparticles and basefluid densities. The nanoparticles increase the density of the basefluid since the solid has a higher density than the liquid. The density of NF is an essential property because it affects the Reynolds number, friction factor, pressure drop, and Nu number. Fig. 4b presents the experimental data of density for Al_2O_3, and TiO_2 NFs in the range of 20 °C–70 °C at varying volume fraction (0.05 & 0.3 vol%). As it is portrayed in the figure, the density decreases with the increase of temperature and in all cases, NF gave higher density than the basefluid. Moreover, it has to be said that the NF density increases with the increase of the nanoparticle concentration. It is shown that the TiO_2 NF has a higher density than Al_2O_3 NF. Similar trends were reported in the literature [5,75–77].

Fig. 4c shows the TC of the mixture of DW/EG (50:50), Al_2O_3–DW/EG NF with the characterization of 0.05% volume fraction, pH equals 3.66 and Al_2O_3–DW/EG NF with the characterization of 0.3% volume fraction, pH equals 9.81 and with the addition of 1:1 nanoparticle to AG surfactant mass ratio. TC of the basefluid in Fig. 4c above was compared with ASHRAE standard [74], and a similar trend for the basefluid was obtained. Moreover, the NFs show that the TC has enhanced after adding nanoparticles to the basefluid and with increasing the volume fraction the TC improved. Also, the highest enhancement of TC was found to be at 65, and 70 °C for the 0.3% volume fraction and the values

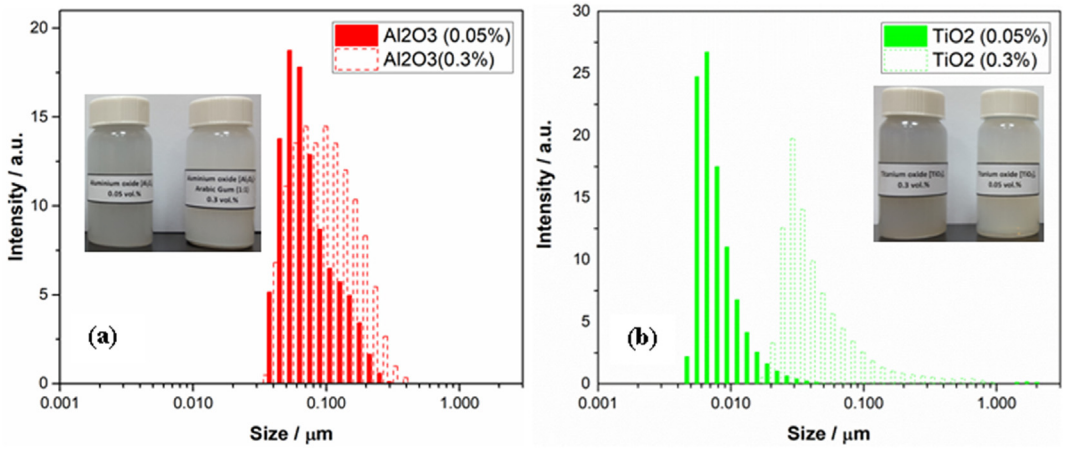

Fig. 3. Particle size distribution of a) Al_2O_3 NFs (inset after 24 h) b) TiO_2 NFs (inset after 24 h).

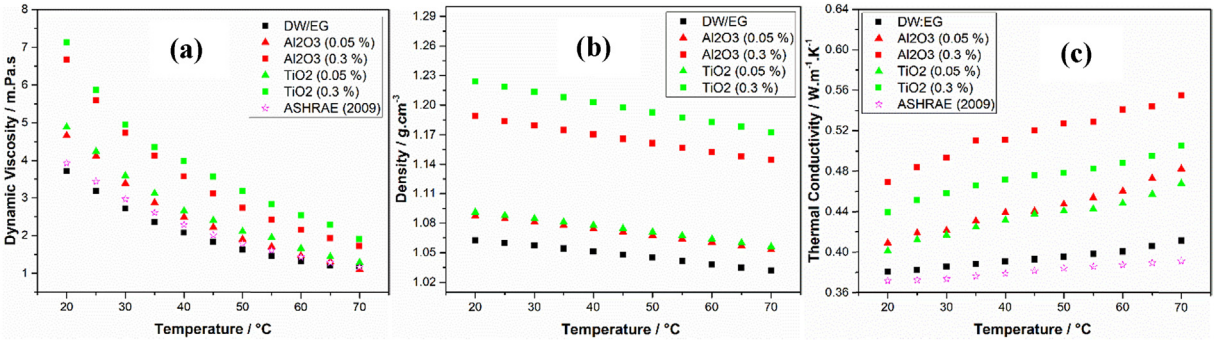

Fig. 4. a) Viscosity of different NFs as a function of temperatures b) Density of different NFs as a function of temperatures [74], and c) Variation of TC with the temperature for DW/EG basefluid, Al_2O_3–DW/EG NF and TiO_2–DW/EG NF at a different volume fractions [74].

of TC was between 0.543 and 0.555 $W\,m^{-1}\,K^{-1}$. It is obvious from Fig. 5c that the TC of TiO_2 NF increased with higher volume fraction from 0.05% to 0.3% and the highest value of TC was found to be around 0.505 $W\,m^{-1}\,K^{-1}$ at 70 °C. Comparing the results of TC of TiO_2 NFs with Al_2O_3 NFs, the TC of Al_2O_3 NF at 0.3% volume fraction had a better improvement rather than TiO_2 NFs. The increased TC is due to Brownian motion, are the main factors that control the thermal behavior of nanoparticles in the basefluid. The TC of the NF increases with increasing the temperature and volume concentration, while it decreases with increasing of the particle size [5].

3.4. Corrosion test results

The corrosion rates were measured on three copper samples using a Biologic workstation coupled with EC-Lab software. Fig. 5a depicts the current-voltage profiles in semi-log scale for the studied samples in an acidic environment. It is clear that the reference specimen (see inset in Fig. 5a) that was tested in 0.5 mol L^{-1} HCl without the addition of any nanoparticles is the most damaged one. Furthermore, the specimen that was tested in the same acidic electrolyte with the addition of TiO_2 at 0.05% (same pH as the reference) seems to be the least corroded one. The corrosion rate in mm per year (mmpy), $E_{corr,}$ and I_{corr} obtained from Fig. 5a using Tafel fit approximation are presented in Table 5.

The fitting corrosion parameters confirm that the sample tested using TiO_2 nanoparticles has the lowest I_{corr} of 4.82 μA which indicates a minimum electrochemical reactivity. However, when the Al_2O_3 nanoparticles were added to the electrolyte, E_{crorr} decreased by 20 mV which means that it is more favorable thermodynamically. The effect of the corrosive properties of the NFs was also investigated. The results in

Table 5
E_{corr}, I_{corr} and corrosion rate for the tested samples.

	Sample	E_{corr} (mV)	I_{corr} (μA)	Corrosion Rate (mmpy)
Acidic medium	Reference	−304.80	7.38	0.172
	TiO_2	−306.46	4.82	0.112
	Al_2O_3	−326.85	5.70	0.133
	Reference	−34.823	0.098	0.022
NF	TiO_2	−265.060	41.88	0.976
	Al_2O_3	59.489	1.261	0.029

Fig. 5b which are carried out using fresh copper samples as working electrodes immersed in the basefluid as well as in the two Al_2O_3 and TiO_2-based NFs show the opposite behavior to that shown in Fig. 5a. This indicates that Al_2O_3-based NF is less corrosive for the piping system in heating applications. This is due to the difference in the pH value of the NFs, which is pH 9.81 for Al_2O_3 based NF and pH equals 3.66 for TiO_2-based NFs.

3.5. Radiator test results

The experimental runs on the radiator were done for five different types of coolants: **(i)** basefluid (50:50 DW/EG) **(ii)** Al_2O_3 and TiO_2 based NFs at 0.05 vol% (i.e., 0.19 wt% for Al_2O_3 and 0.18 wt% for TiO_2), and (iii) Al_2O_3 and TiO_2 based NFs at 0.3 vol% (i.e. 1.02 wt% for Al_2O_3 and 1.12 wt% for TiO_2). The amount of coolant was set to 4 L placed in a reservoir tank (see Fig. 1), and heated to 80 °C. After reaching 80 °C, the pump and the fan were switched on. The tests were done for four different flow rates (0.5, l, 2 and 3 L min^{-1}) for 30 min each. The temperatures were recorded every 1 s using a data logger

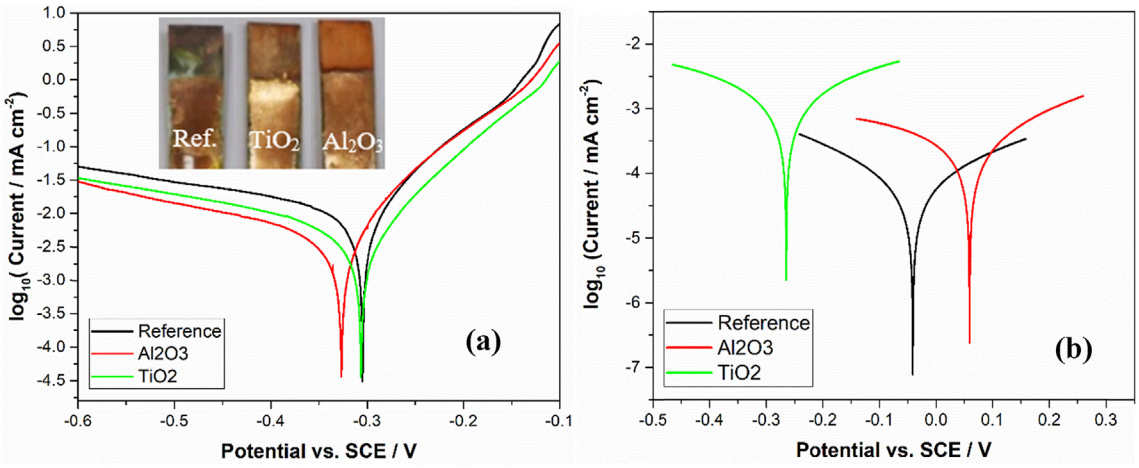

Fig. 5. a) The three copper specimens: 0.5 M HCL as a reference, 0.5 M HCL + Al_2O_3 nanoparticles, and 0.5 M HCL + TiO_2 nanoparticles b) The E_{we} with the log I for the three tested samples.

(Graphtec GL240, for K type thermocouples ± (0.05% of rdg. +1.0).

Fig. 6 shows the experimental Nu number values vs. flow rate computed for the five studied coolants. Prior to analyzing the Nu number (eq. (1)), Fig. 6 showed that the optimum flow rate is about 1 L min^{-1} (results are not shown here). Generally, higher flow rates increase the heat transfer, but after a certain limit, the fluid does not remain for an adequate time in the system for the heat transfer to be properly performed. Nu, on the other hand, is a nondimensional heat transfer coefficient which gives an appropriate comparison between the conduction and convection heat transfer. From Fig. 6, it can be said that the use of NFs enhances the performance of the radiator setup at all tested flow rates. The flow structure is affected by the presence of the nanoparticles in the basefluid, therefore chaotic movements, dispersions and fluctuations of the nanoparticles especially near the tube wall result in enhanced energy exchange rates between the tube wall and the fluid. Furthermore, the increase in the concentration of nanoparticles (see for instance Nu increases from 6.78% to 23.67% as the concentration increases from 0.05 vol% to 0.3 vol%, shown in Fig. 6.) increases the heat transfer performance due to increased TC. This is due to the increased interaction and collision of nanoparticles which intensify even more with the increase in volume fraction resulting in enhanced heat transfer from the tube wall to the NF [78]. As for the difference between the two types of NFs, Al_2O_3 based one outperforms TiO_2 NF in terms of heat transfer enhancement: for example, for 1 L min^{-1} flowrate, the Nu number for Al_2O_3 at 0.05 vol% was 9.79% higher than the reference, and 24.21% higher when 0.3 vol% was used. Whereas, the enhancement of Nu for TiO_2 at 0.05 vol% and 0.3 vol% was 5.73% and 14.99% for the mass flow rate of 1 L min^{-1}, respectively. These results are in line with recent literature; Hwang et al. [79] reported an enhancement in Nu above 8% at 0.3 vol% of Al_2O_3 nanoparticles under laminar condition. Xuan and Li [80] investigated Cu nanoparticles in DW and showed that the Nu for the NF flowing in a tube under constant wall heat flux varied from 5% to 14% by increasing the volume fraction from 0.5% to 1.2% for the same flow rate, respectively. Peyghambarzadeh et al. [81] reported an enhancement of 40% in Nu number using 1 vol% of Al_2O_3 nanoparticles into DW or EG in comparison with the pure DW and pure EG, and Suresh et al. [82] reported an increase of 13.56% in Nu number using 0.1 vol% of Al_2O_3–Cu/water hybrid NFs. This result was expected due to the higher TC of Al_2O_3 nanoparticles presented in Table 3.

The efficiency of the automotive radiators is effected by the Pumping power. For this purpose, the friction factor is analyzed under similar conditions as those used for the overall heat transfer coefficient. Fig. 7a shows the effect of volume fraction on the friction factor for both the investigated NFs as well as the basefluid. It can be said that the trends of the points in Fig. 7a are similar to the results of equation (5) about the friction factor. The mass flow rate of the hot fluid flowing in the tubes of the radiators is directly proportional to the pumping power. Increased mass flow rate results in increased Reynolds number which results in higher head loss due to the friction in riser tubers and head loss due to sudden expansion and contraction in header tube. Consequently, pumping power increases since the head losses are increasing. The friction factor at 70 °C decreased by 1.80%, 1.80%, 1.80% and 0.59% for 0.05 vol% and 14.74%, 14.74%, 14.74% and 5.00% for 0.3 vol% of Al_2O_3 NFs at the mass flow rates of 0.5, 1, 2, and 3 L min^{-1}, and for TiO_2 NFs it increased by 2.41%, 2.41%, 2.41% and 0.78% for 0.05 vol% and decreased by 10.03%, 10.03%, 10.03% and 3.36% for 0.3 vol% at the same mass flow rates. The same findings have been reported in the literature for laminar and turbulent flow regimes [52,62,82,83].

The PEC is directly related to the gains and losses of energy in an industrial plant. Such criteria have already been used by other researchers [60,84,85]. As for the heat transfer coefficient where the Nu has been compared with that of basefluid, similarly, the PEC ratio for the four NFs presented in Fig. 7b. The PEC values at 70 °C reaches a maximum of 110% and 131% for the volume fractions of 0.05% and 0.3% for Al_2O_3 NFs at a flow rate of 1 L min^{-1}, and for TiO_2 NFs at the same volume fractions and flow rate, the PEC values reaches a maximum of 107% and 122% for 0.5 and 1 L min^{-1}, respectively. From the PEC values of the studied fluid, it appears that the energy budget using NFs is favorable. The volume fraction increases the friction factor and pumping power slightly; this increase is due to the addition of the nanoparticles to the basefluid, which results in higher density as well as the higher viscosity of the NFs. Similar trends were reported by other literature studies [5,65,86].

3.6. Re-evaluation of some NFs properties after radiator tests

Fig. 8 represents the NFs at a volume fraction of 0.3% before and after being used in a radiator for a period of 6 months. It can be observed from the figure that Al_2O_3 NF after being used in a radiator and tested after a period of 6 months showed an increment in the average particle diameter from 0.086 μm (86 nm) to 0.765 μm (765 nm), which means that the particles have aggregated and thus showing bigger sized particles. For TiO_2 NF after being used in a radiator and test after a period of 6 months showed an increment as well in the average particle diameter from 0.036 μm (36 nm) to two peaks of 0.0688 μm (68.8 nm) and 0.659 μm (659 nm), which showed an aggregation of the nanoparticles as well but smaller compared to Al_2O_3 NF.

The TC of Al_2O_3 NF and TiO_2 NF at 0.3% volume fractions after being used in a car radiator versus the initially prepared NFs are shown in Fig. 9. It is observed from the data that TC values for Al_2O_3 NF have dropped significantly by 5.46%, 6.92%, 5.73%, 3.48% and 4.28% for the temperatures of 25 °C, 35 °C, 45 °C, 55 °C, and 65 °C, however, TiO_2 NF after being used in the radiator dropped by 0.82%, 1.59%, 1.83%, 0.25% and 0.81% which is not very high compared to Al_2O_3 NF. Hence it could be concluded from this results reported in Fig. 8, that the thermophysical properties of prepared NFs might show improved and better results in the short period, but for the long run, it may not stay the same. In this study, Al_2O_3 NF showed better properties and heat transfer enhancement in the short run, but comparing the TC property which is the main contributing property regarding heat transfer enhancement dropped significantly after being used in a radiator. However, TiO_2 NF showed consistent values with a slight drop compared to the initial values of TC, this can also be verified from the particle size distribution shown in Fig. 8. Which shows that the particle size of the Al_2O_3 NF has become larger, therefore, making the NF less stable

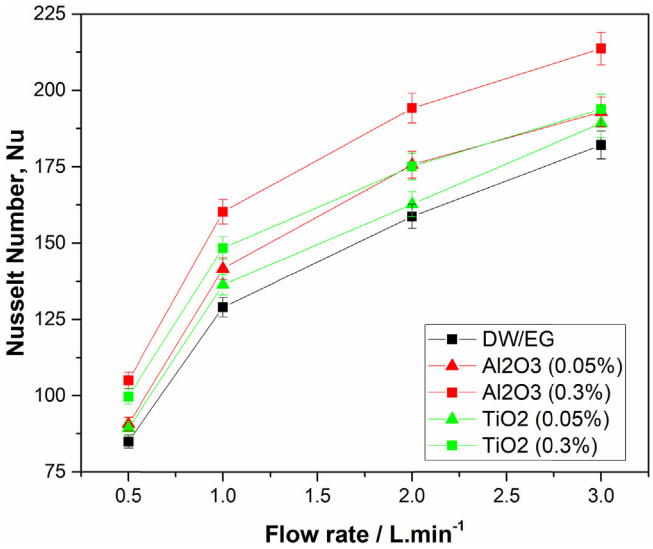

Fig. 6. Radiator performance comparison using NF (0.05%, 0.3%, and basefluid) with respect to the effect of volume concentration on the Nu number at different flow rates.

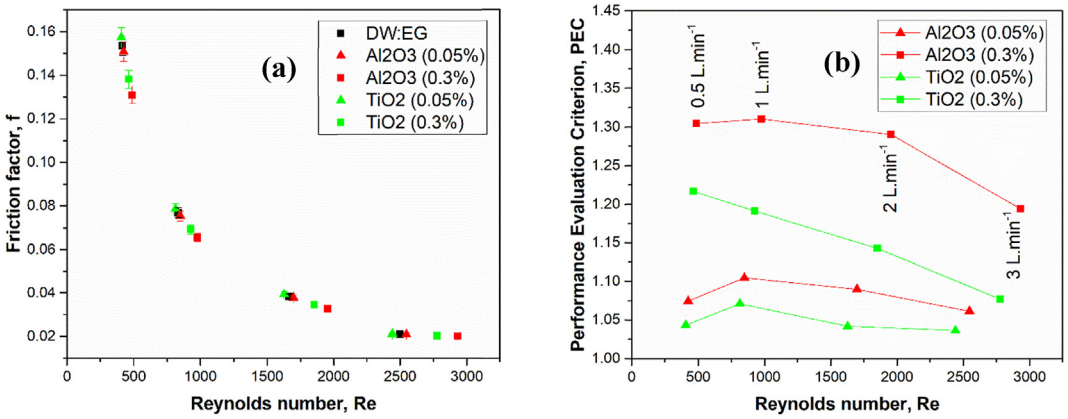

Fig. 7. Effect of volume fraction and flow rates on (a) the friction factor and (b) PEC with respect to Reynolds number.

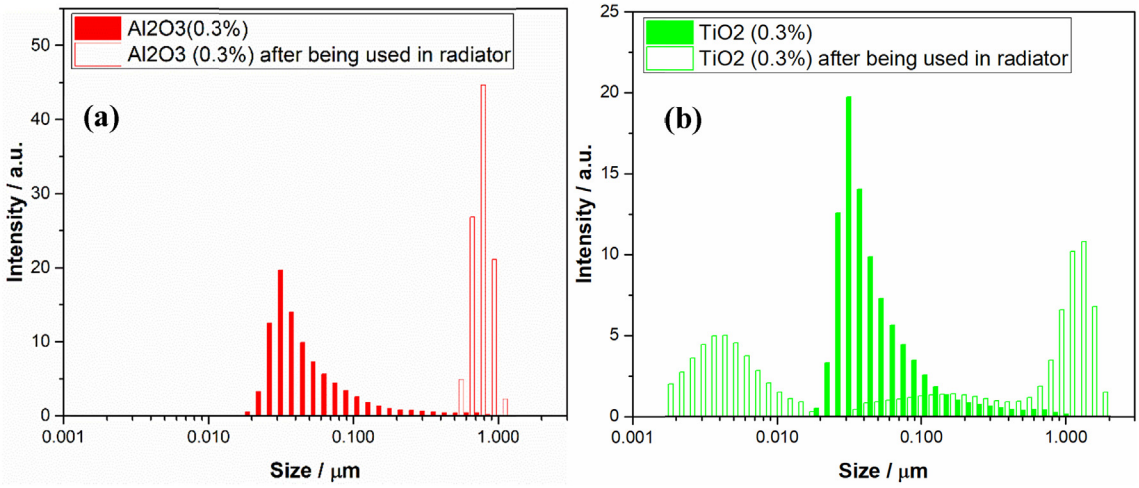

Fig. 8. Particle size distribution of (a) Al_2O_3 NFs (b) TiO_2 NFs, before and after being used in a car radiator.

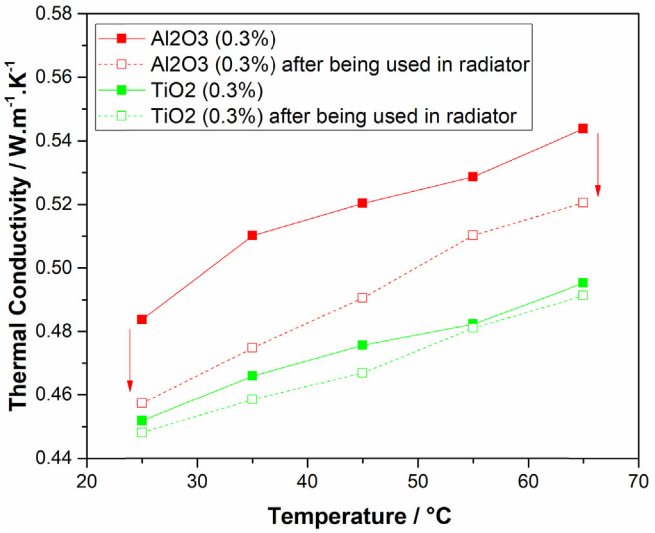

Fig. 9. TC with the temperature for Al_2O_3–DW/EG NF and TiO_2–DW/EG NF at 0.3% volume fractions before and after being used in a car radiator after 6 months.

compared to the TiO_2 NF which resulted in better size range and TC after being used in the system, making it a better coolant in the long run." The drop in the thermal conductivity of Al_2O_3 NF could also be due to the use of AG surfactants, as reported elsewhere [5,7], which has a lower melting temperature [87] and which effects the stability of NFs at higher temperatures. The behavior was observed for the studied NF as a surfactant was used to ensure the stability of the prepared Al_2O_3 NF.

More research with a broader range of particle loadings in the various basefluid is required to see the tribological effect in automotive thermal systems. Nanoparticles suspended in coolant has the perspective to enhance cooling rates of an automotive and heavy-duty engine with a compact sized cooling system. Further extensive investigations in this area will contribute to the design of efficient engine cooling and other thermal systems that contain NFs. Advance cooling system design using NFs would create a future generation engine that would work at higher optimum temperatures with improved power output. Higher speeds, better fuel consumption, reduced environmental impact and reduction in cost can be achieved with lighter and smaller engine components. So, the future engines with nanofluids can be more efficient and more sustainable energy systems which will lead to reducing environmental issues such as global warming [88,89]. It is also very important to develop a common correlation for NF heat transfer and friction factor in radiators. Therefore, additional investigations are required to develop generalized Nu and friction factor corrections for NFs in automotive applications. The improvement of the heat transfer ability of the NFs also makes their use in heat exchangers an interesting option, resulting in better system performance with an added advantage in energy efficiency.

4. Conclusions

The objective of this paper is to carry out an experimental investigation of the heat transfer in an actual automobile radiator which operates with different nanofluids. The examined nanofluids are created by dispersing Al_2O_3 and TiO_2 nanoparticles in DW and EG at 50:50 mixtures by volume and the analysis is conducted for different volume fractions and flow rates. The TiO_2–DW/EG NFs and Al_2O_3–DW/EG NFs were prepared by using a two-step method. The thermophysical properties of the examined NFs have been studied in this paper in order to determine their impact on the heat transfer phenomena. Their stability was also examined using ζ-method and particle size analysis, while a corrosion test had been also done for copper samples. The most important conclusions of this work are summarized below:

- The most stable sample from Al_2O_3 NFs was Al_2O_3–DW/EG NFs at 0.3% volume fraction with 1:1 nanoparticle to AG surfactant mass ratio. As for the TiO_2 NFs, the TiO_2 -DW/EG NFs with 0.3% volume fraction without any addition of surfactant was found to be the most stable nanofluid.
- The dynamic light scattering results show that the high volume concentration leads to an increase in the average particle size which is not good for the stability of nano-suspension.
- The viscosity and density results show that TiO_2 NF has higher viscosity and density compared to Al_2O_3 NFs, while the TC of Al_2O_3–DW/EG NF at 0.3% volume fraction had a better performance than TiO_2 –DW/EG NFs.
- The highest Nu was found to be at 0.3% volume fraction for all measured flow rates and from corrosion test. The corrosion test showed that Al_2O_3 nanoparticles have a higher corrosion rate (0.133 mmpy) than TiO_2 nanoparticles (0.112 mmpy) in an acidic electrolyte. However, Al_2O_3-based NF showed lower corrosion (0.029 mmpy) for the piping system compared to TiO_2-based NF (0.976 mmpy) in heating applications.
- Finally, it is significant to state that the Nusselt number increases with the use of nanoparticles and especially for the Al_2O_3 nanoparticle. The enhancement is found 9.79% with 0.05% concentration and 24.21% with 0.3% concentration at a mass flow rate of 1 L min^{-1}.

The findings of this study can be easily scaled up and used for automotive car radiators for better performance. Moreover, this work suggests future directions for engineers to manufacture extremely compressed and effective radiators for automotive.

Acknowledgments

The University of Sharjah financially supported this work, Projects #18020406118. Also, Dr. E. Bellos would like to thank “Bodossaki Foundation” for its financial support. The first author would also like to thank Amel Mohammed Abdullah for her assistance.

References

[1] Mukkamala Y. Contemporary trends in thermo-hydraulic testing and modeling of automotive radiators deploying nano-coolants and aerodynamically efficient air-side fins. Renew Sustain Energy Rev 2017;76:1208–29.
[2] Alam T, Kim M-H. A comprehensive review on single phase heat transfer enhancement techniques in heat exchanger applications. Renew Sustain Energy Rev 2018;81:813–39.
[3] Bigdeli MB, et al. A review on the heat and mass transfer phenomena in nanofluid coolants with special focus on automotive applications. Renew Sustain Energy Rev 2016;60:1615–33.
[4] Mannekote JK, et al. Environmentally friendly functional fluids from renewable and sustainable sources-A review. Renew Sustain Energy Rev 2018;81:1787–801.
[5] Gupta M, et al. A review on thermophysical properties of nanofluids and heat transfer applications. Renew Sustain Energy Rev 2017;74:638–70.
[6] Zhao N, Li S, Yang J. A review on nanofluids: data-driven modeling of thermal-physical properties and the application in automotive radiator. Renew Sustain Energy Rev 2016;66:596–616.
[7] Gupta M, et al. Up to date review on the synthesis and thermophysical properties of hybrid nanofluids. J Clean Prod 2018;190:169–92.
[8] Sidik NAC, Yazid MNAWM, Mamat R. Recent advancement of nanofluids in engine cooling system. Renew Sustain Energy Rev 2017;75:137–44.
[9] Tawfik MM. Experimental studies of nanofluid thermal conductivity enhancement and applications: a review. Renew Sustain Energy Rev 2017;75:1239–53.
[10] Said Z, et al. Evaluating the optical properties of TiO2 nanofluid for a direct absorption solar collector. Numer Heat Tran, Part A: Applications 2015;67(9):1010–27.
[11] Xuan Y, Roetzel W. Conceptions for heat transfer correlation of nanofluids. Int J Heat Mass Transf 2000;43(19):3701–7.
[12] Maiga SEB, et al. Heat transfer enhancement by using nanofluids in forced convection flows. Int J Heat Fluid Flow 2005;26(4):530–46.
[13] Said Z, et al. Acid-functionalized carbon nanofibers for high stability, thermo-electrical and electrochemical properties of nanofluids. J Colloid Interface Sci 2018;520:50–7.
[14] Kakaç S, Pramuanjaroenkij A. Review of convective heat transfer enhancement with nanofluids. Int J Heat Mass Transf 2009;52(13–14):3187–96.
[15] Das SK, et al. Nanofluids: science and technology. John Wiley & Sons; 2007.
[16] Rashmi W, et al. Investigating corrosion effects and heat transfer enhancement in smaller size radiators using CNT-nanofluids. J Mater Sci 2014;49(13):4544–51.
[17] Alawi OA, et al. Thermal conductivity and viscosity models of metallic oxides nanofluids. Int J Heat Mass Transf 2018;116:1314–25.
[18] Koca HD, et al. Effect of particle size on the viscosity of nanofluids: a review. Renew Sustain Energy Rev 2017;82:1664–74.
[19] Dardan E, Afrand M, Isfahani AM. Effect of suspending hybrid nano-additives on rheological behavior of engine oil and pumping power. Appl Therm Eng 2016;109:524–34.
[20] Ambreen T, Kim M-H. Heat transfer and pressure drop correlations of nanofluids: a state of art review. Renew Sustain Energy Rev 2018;91:564–83.
[21] Prasher R, et al. Measurements of nanofluid viscosity and its implications for thermal applications. Appl Phys Lett 2006;89(13):133108.
[22] Raja M, et al. Review on nanofluids characterization, heat transfer characteristics and applications. Renew Sustain Energy Rev 2016;64:163–73.
[23] Kumar DD, Arasu AV. A comprehensive review of preparation, characterization, properties and stability of hybrid nanofluids. Renew Sustain Energy Rev 2018;81:1669–89.
[24] Das PK, et al. Synthesis and characterization of TiO 2–water nanofluids with different surfactants. Int Commun Heat Mass Transf 2016;75:341–8.
[25] Said Z, et al. Performance enhancement of a flat plate solar collector using titanium dioxide nanofluid and polyethylene glycol dispersant. J Clean Prod 2015;92:343–53.
[26] Khairul M, et al. Effects of surfactant on stability and thermo-physical properties of metal oxide nanofluids. Int J Heat Mass Transf 2016;98:778–87.
[27] Witharana S, et al. Stability of glycol nanofluids—the theory and experiment. Powder Technol 2013;239:72–7.
[28] Li X, et al. Thermal conductivity enhancement dependent pH and chemical surfactant for Cu-H 2 O nanofluids. Thermochim Acta 2008;469(1):98–103.
[29] Goudarzi K, Jamali H. Heat transfer enhancement of Al 2 O 3-EG nanofluid in a car radiator with wire coil inserts. Appl Therm Eng 2017;118:510–7.
[30] Naik M, et al. Experimental investigation into rheological property of copper oxide nanoparticles suspended in propylene glycol-water based fluids. 2010.
[31] Kim HJ, Bang IC, Onoe J. Characteristic stability of bare Au-water nanofluids fabricated by pulsed laser ablation in liquids. Optic Laser Eng 2009;47(5):532–8.
[32] Abdul Hamid K, et al. Thermal conductivity enhancement of TiO2 nanofluid in water and ethylene glycol (EG) mixture. Indian J Pure Appl Phys 2016;54(10):651–5.
[33] Drzazga M, et al. Preparation of metal oxide-water nanofluids by two-step method. Inż. Ap. Chem 2012;51:213–5.
[34] Rudyak VY, Minakov AV. Thermophysical properties of nanofluids. The European Physical Journal E 2018;41(1):15.
[35] Murshed S, et al. Morphology and thermophysical properties of non-aqueous titania nanofluids. Heat Mass Transf 2018:1–6.
[36] Philip J, Shima P. Thermal properties of nanofluids. Adv Colloid Interface Sci 2012;183:30–45.
[37] Amani M, et al. Multi-objective optimization of thermophysical properties of eco-friendly organic nanofluids. J Clean Prod 2017;166:350–9.
[38] Khanafer K, Vafai K. A review on the applications of nanofluids in solar energy field. Renew Energy 2018;123:398–406.
[39] Wong KV, De Leon O. Applications of nanofluids: current and future. Adv Mech Eng 2010;2:519659.
[40] Rashidi S, Mahian O, Languri EM. Applications of nanofluids in condensing and evaporating systems. J Therm Anal Calorim 2018;131(3):2027–39.
[41] De Leon O, Wong KV. Applications of nanofluids: current and future. Nanotechnology and energy. Pan Stanford; 2017. p. 105–32.
[42] Leong K, et al. Performance investigation of an automotive car radiator operated with nanofluid-based coolants (nanofluid as a coolant in a radiator). Appl Therm Eng 2010;30(17):2685–92.
[43] Heris SZ, et al. Experimental study of heat transfer of a car radiator with CuO/ethylene glycol-water as a coolant. J Dispersion Sci Technol 2014;35(5):677–84.
[44] Celata GP, et al. Experimental results of nanofluids flow effects on metal surfaces. Chem Eng Res Des 2014;92(9):1616–28.
[45] Naraki M, et al. Parametric study of overall heat transfer coefficient of CuO/water nanofluids in a car radiator. Int J Therm Sci 2013;66:82–90.
[46] Li X, Zou C, Qi A. Experimental study on the thermo-physical properties of car

engine coolant (water/ethylene glycol mixture type) based SiC nanofluids. Int Commun Heat Mass Transf 2016;77:159–64.
[47] Devireddy S, Mekala CSR, Veeredhi VR. Improving the cooling performance of automobile radiator with ethylene glycol water based TiO 2 nanofluids. Int Commun Heat Mass Transf 2016;78:121–6.
[48] Elsebay M, et al. Numerical resizing study of Al 2 O 3 and CuO nanofluids in the flat tubes of a radiator. Appl Math Model 2016;40(13):6437–50.
[49] Chiam H, et al. Thermal conductivity and viscosity of Al2O3 nanofluids for different based ratio of water and ethylene glycol mixture. Exp Therm Fluid Sci 2017;81:420–9.
[50] Gulhane A, Chincholkar S. Experimental investigation of convective heat transfer coefficient of Al2O3/water nanofluid at lower concentrations in a car radiator. Heat Transf Asian Res 2017;46(8):1119–29.
[51] Hatami M, et al. Investigation of engines radiator heat recovery using different shapes of nanoparticles in H 2 O/(CH 2 OH) 2 based nanofluids. Int J Hydrogen Energy 2017;42(16):10891–900.
[52] Hussein AM, Bakar R, Kadirgama K. Study of forced convection nanofluid heat transfer in the automotive cooling system. Case Studies in Thermal Engineering 2014;2:50–61.
[53] Oliveira GA, Contreras EMC, Bandarra Filho EP. Experimental study on the heat transfer of MWCNT/water nanofluid flowing in a car radiator. Appl Therm Eng 2017;111:1450–6.
[54] Selvam C, Lal DM, Harish S. Enhanced heat transfer performance of an automobile radiator with graphene based suspensions. Appl Therm Eng 2017;123:50–60.
[55] Geehan G, Ritika R, Winchester C. Impact of nanofluids and specific frequency absorbers in parabolic trough collector solar furnaces. PAM Review: Energy Sci Technol 2018;5:89–103.
[56] Hawwash A, et al. Experimental study of alumina nanofluids effects on thermal performance efficiency of flat plate solar collectors. GSTF J Eng Technol 2017;4(1).
[57] Esfe MH, Firouzi M, Afrand M. Experimental and theoretical investigation of thermal conductivity of ethylene glycol containing functionalized single walled carbon nanotubes. Phys E Low-dimens Syst Nanostruct 2018;95:71–7.
[58] Kartikawati NA, et al. Measurement and correlation of the physical properties of aqueous solutions of ammonium based ionic liquids. J Mol Liq 2018;253:250–8.
[59] Amrutkar, P. and S. Patil, Automotive radiator sizing and rating–Simulation approach. IOSR J Mech Civ Eng: p. 1-5.
[60] Pak BC, Cho YI. Hydrodynamic and heat transfer study of dispersed fluids with submicron metallic oxide particles. Experimental Heat Transfer an International Journal 1998;11(2):151–70.
[61] Li Q, Xuan Y. Convective heat transfer and flow characteristics of Cu-water nanofluid. Sci China E 2002;45(4):408–16.
[62] Abdolbaqi MK, et al. Experimental investigation and development of new correlations for heat transfer enhancement and friction factor of BioGlycol/water based TiO2 nanofluids in flat tubes. Int J Heat Mass Transf 2017;108:1026–35.
[63] Reddy MCS, Rao VV. Experimental investigation of heat transfer coefficient and friction factor of ethylene glycol water based TiO2 nanofluid in double pipe heat exchanger with and without helical coil inserts. Int Commun Heat Mass Transf 2014;50:68–76.
[64] Xuan Y, Li Q. Investigation on convective heat transfer and flow features of nanofluids. J Heat Transf 2003;125(1):151–5.
[65] Vajjha RS, Das DK, Namburu PK. Numerical study of fluid dynamic and heat transfer performance of Al2O3 and CuO nanofluids in the flat tubes of a radiator. Int J Heat Fluid Flow 2010;31(4):613–21.
[66] Filonenko G. Hydraulic resistance in pipes. Teploenergetika 1954;1:40–4.
[67] Beckwith TG, Buck NL, Marangoni RD. Mechanical measurements vol. 5. Reading, MA: Addison-Wesley; 1969.
[68] Webb R. Performance evaluation criteria for use of enhanced heat transfer surfaces in heat exchanger design. Int J Heat Mass Transf 1981;24(4):715–26.
[69] Said Z, Kamyar A, Saidur R. Experimental investigation on the stability and density of TiO2, Al2O3, SiO2 and TiSiO4. IOP conference series: earth and environmental science. IOP Publishing; 2013.
[70] Krishnakumar T, Viswanath S, Varghese SM. Experimental studies on thermal and rheological properties of Al2O3–ethylene glycol nanofluid. Int J Refrig 2018;89:122–30.
[71] Sajid MU, Ali HM. Recent advances in application of nanofluids in heat transfer devices: a critical review. Renew Sustain Energy Rev 2019;103:556–92.
[72] Zhai Y, et al. Evaluation of surfactant on stability and thermal performance of Al2O3-ethylene glycol (EG) nanofluids. Powder Technol 2019;343:215–24.
[73] Azman NF, Samion S. Dispersion stability and lubrication mechanism of nanolubricants: a review. International Journal of Precision Engineering and Manufacturing-Green Technology 2019:1–22.
[74] ASHRAE H-F, Atlanta G. American society of heating. Refrigerating and Air-Conditioning Engineers; 2009.
[75] Elias M, et al. Experimental investigation on the thermo-physical properties of Al 2 O 3 nanoparticles suspended in car radiator coolant. Int Commun Heat Mass Transf 2014;54:48–53.
[76] Said Z, Saidur R. Thermophysical properties of metal oxides nanofluids. Nanofluid heat and mass transfer in engineering problems. InTech; 2017.
[77] Said Z, et al. Experimental investigation of the thermophysical properties of AL2O3-nanofluid and its effect on a flat plate solar collector. Int Commun Heat Mass Transf 2013;48:99–107.
[78] Heris SZ, Esfahany MN, Etemad SG. Experimental investigation of convective heat transfer of Al2O3/water nanofluid in circular tube. Int J Heat Fluid Flow 2007;28(2):203–10.
[79] Hwang KS, Jang SP, Choi SU. Flow and convective heat transfer characteristics of water-based Al2O3 nanofluids in fully developed laminar flow regime. Int J Heat Mass Transf 2009;52(1–2):193–9.
[80] Xuan Y, Li Q. Heat transfer enhancement of nanofluids. Int J Heat Fluid Flow 2000;21(1):58–64.
[81] Peyghambarzadeh S, et al. Experimental study of heat transfer enhancement using water/ethylene glycol based nanofluids as a new coolant for car radiators. Int Commun Heat Mass Transf 2011;38(9):1283–90.
[82] Suresh S, et al. Effect of Al2O3–Cu/water hybrid nanofluid in heat transfer. Exp Therm Fluid Sci 2012;38:54–60.
[83] Redhwan A, et al. Comparative study of thermo-physical properties of SiO2 and Al2O3 nanoparticles dispersed in PAG lubricant. Appl Therm Eng 2017;116:823–32.
[84] Maré T, et al. Comparison of the thermal performances of two nanofluids at low temperature in a plate heat exchanger. Exp Therm Fluid Sci 2011;35(8):1535–43.
[85] Ferrouillat S, et al. Influence of nanoparticle shape factor on convective heat transfer and energetic performance of water-based SiO2 and ZnO nanofluids. Appl Therm Eng 2013;51(1–2):839–51.
[86] Pandey SD, Nema V. Experimental analysis of heat transfer and friction factor of nanofluid as a coolant in a corrugated plate heat exchanger. Exp Therm Fluid Sci 2012;38:248–56.
[87] Mothé C, Rao M. Thermal behavior of gum Arabic in comparison with cashew gum. Thermochim Acta 2000;357:9–13.
[88] Said Z, et al. Heat transfer enhancement and life cycle analysis of a Shell-and-Tube Heat Exchanger using stable CuO/water nanofluid. Sustainable Energy Technologies and Assessments 2019;31:306–17.
[89] Said Z, Arora S, Bellos E. A review on performance and environmental effects of conventional and nanofluid-based thermal photovoltaics. Renew Sustain Energy Rev 2018;94:302–16.